

## **Research Paper**

### **Title:**

**Silicon Electrodeposition in Water-soluble KF–KCl Molten Salt:  
Optimization of Electrolysis Conditions at 923 K**

### **Authors:**

**Kouji YASUDA,<sup>a,b,z</sup> Kazuma MAEDA,<sup>a</sup> Toshiyuki NOHIRA,<sup>c,z</sup>**

**Rika HAGIWARA,<sup>a</sup> and Takayuki HOMMA<sup>d</sup>**

### **Affiliation:**

<sup>a</sup>Department of Fundamental Energy Science, Graduate School of Energy Science,  
Kyoto University, Yoshida-hommachi, Sakyo-ku, Kyoto 606-8501, Japan.

<sup>b</sup>Environment, Safety and Health Organization, Kyoto University, Yoshida-  
hommachi, Sakyo-ku, Kyoto 606-8501, Japan.

<sup>c</sup>Institute of Advanced Energy, Kyoto University, Gokasho, Uji 611-0011, Japan.

<sup>d</sup>Faculty of Science and Engineering, Waseda University, 3-4-1 Okubo, Shinjuku-ku,  
Tokyo 169-8555, Japan.

### **<sup>z</sup>Corresponding Authors:**

yasuda.kouji.3v@kyoto-u.ac.jp (K. Yasuda)

nohira.toshiyuki.8r@kyoto-u.ac.jp (T. Nohira)

Tel.: +81-75-753-4817; Fax: +81-75-753-5906.

## Abstract

To establish a new Si-electrodeposition process, the optimum conditions for obtaining adherent, compact, and smooth Si films using molten KF–KCl–K<sub>2</sub>SiF<sub>6</sub> were investigated at 923 K. Galvanostatic electrolysis was conducted on a Ag substrate in eutectic KF–KCl (45:55 mol%) with various current densities (10–500 mA cm<sup>-2</sup>) and K<sub>2</sub>SiF<sub>6</sub> concentrations (0.5–5.0 mol%). Cross-sectional scanning electron microscopy (SEM) of the deposits revealed that compact and smooth Si films form at intermediate K<sub>2</sub>SiF<sub>6</sub> concentrations and current densities. The relationship between the deposition conditions and Si morphology is discussed in terms of the electrodeposition mechanism.

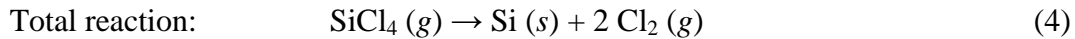
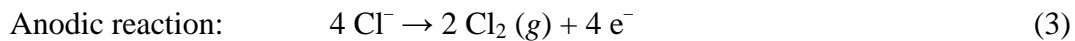
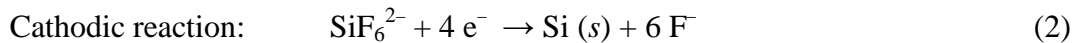
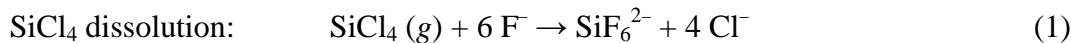
## 1. Introduction

Photovoltaic power generation is attracting substantial attention as an environmentally friendly renewable energy. Until now, the prevalent material for solar cells has been silicon, particularly polycrystalline and single-crystalline Si. Currently, polycrystalline Si for solar cells is produced by slicing high-purity Si ingots prepared using the Siemens process. However, the low productivity of the Siemens process and the considerable kerf loss in the Si-slicing process are the main drawbacks of the conventional production process in terms of energy efficiency and yield. Thus, an efficient process for manufacturing polycrystalline Si for solar cells is required.

The electrodeposition of Si from purified Si compounds is a promising alternative method for producing polycrystalline Si films for solar cells. According to the literature, only amorphous Si is electrodeposited in organic solvents [1,2] and ionic liquids [3,4]. The electrodeposition of crystalline Si from high-temperature molten salts has been reported since the 1970s. Elwell *et al.* obtained a compact and smooth Si layer in molten LiF–NaF–KF at 1018 K [5–9]. Cohen *et al.* also achieved compact and smooth Si deposition in LiF–KF at 1023 K [10]. However, the removal of the adhered salt from the deposited Si was difficult because of the low solubilities of LiF and NaF in water [11]. Among alkali and alkali earth fluorides, KF has exceptionally high solubility in water: 101.6 g (100 g-H<sub>2</sub>O)<sup>−1</sup>. The use of a single KF molten salt is, however, rather difficult because of the high melting point of KF (1131 K). Because KCl also has high solubility in water, low-temperature electrolysis and easy removal of the adhered salt by washing with water can be achieved with a KF–KCl binary system (melting point = 878 K at

eutectic composition [12]) as an electrolyte. Previously, Si electrodeposition was reported by Andriiko *et al.*, who used molten KF–KCl–K<sub>2</sub>SiF<sub>6</sub> (45.8:48.2:6.0 mol%) containing SiO<sub>2</sub> as the main Si source [13]. However, the resulting deposit contained only 20–50 wt% of powder-like Si. Moreover, the addition of SiO<sub>2</sub> requires the elimination of O<sup>2-</sup> ions from the melt. The elimination of O<sup>2-</sup> ions is only practically possible with carbon anodes in molten fluorides, which inevitably results in carbon contamination of the Si deposit because of the formation of CO<sub>3</sub><sup>2-</sup> ions.

Recently, we proposed a novel Si-electrodeposition process utilizing high-purity SiCl<sub>4</sub>, which is commercially available at low cost, as a Si-ion source and KF–KCl mixed molten salt as an electrolyte [14–16]. In this technique, gaseous SiCl<sub>4</sub> is introduced into the molten salt to produce Si(IV) complex ions. Si films are then electrodeposited onto a cathode of an appropriate material, and Cl<sub>2</sub> gas is evolved at a carbon anode. The salt adhered on the Si deposit can be easily removed by washing with water.



In this process, Si electrodeposition is achieved without introducing impurities or changing the composition of the molten salt. Moreover, when the Cl<sub>2</sub> gas by-product is recovered for the chlorination of Si to produce SiCl<sub>4</sub>, a circulation cycle generating no by-product is realized. In our previous studies [14–16], the electrodeposition of Si from Si(IV) complex ions on a Ag electrode at 923 K was investigated in a molten KF–KCl–

$\text{K}_2\text{SiF}_6$  system containing the same Si(IV) complex ions as the introduced  $\text{SiCl}_4$ . The reduction observed as a single 4-electron wave in cyclic voltammetry, was suggested to proceed through an  $\text{E}_\text{q}\text{E}_\text{r}$  (quasireversible-reversible electron transfer reaction) mechanism [16]. The diffusion coefficient of the Si(IV) ions was determined to be  $3.2 \times 10^{-5} \text{ cm}^2 \text{ s}^{-1}$  at 923 K [16].

The present study investigated the effects of  $\text{K}_2\text{SiF}_6$  concentration and current density on the morphology of the Si deposits in molten  $\text{KF-KCl-K}_2\text{SiF}_6$  at 923 K, which are indispensable because the industrial electrolytic processes are conducted under the controlled ion concentration and current. Galvanostatic electrolysis was conducted with various  $\text{K}_2\text{SiF}_6$  concentrations (0.5–5.0 mol%) and current densities ( $10\text{--}500 \text{ mA cm}^{-2}$ ). The optimum conditions for forming adherent, compact, and smooth Si films were discussed based on scanning electron microscopy (SEM) of the Si deposits. Furthermore, the purity of the Si deposits was analyzed by glow discharge mass spectroscopy (GD-MS).

## 2. Experimental

The experimental setup is described elsewhere [16]. The electrochemical experiments were performed in a dry Ar atmosphere at 923 K. Reagent-grade KF and KCl were mixed to the eutectic composition ( $\text{KF}:\text{KCl} = 45:55 \text{ mol\%}$ , melting point = 878 K [12]) and loaded into a graphite crucible. The crucible was placed at the bottom of a quartz vessel in an air-tight Kanthal container and dried under vacuum at 673 K for 24 h. A Ag wire (Nilaco Corp., > 99.99%, diameter: 1.0 mm), a Ag flag electrode (Nilaco Corp., 99.98%, thickness: 0.1 mm), and a Ag plate (Nilaco Corp., 99.98%, thickness: 0.2 mm) were used as working electrodes. A glassy carbon rod (Tokai Carbon Co., Ltd.,

diameter: 5.0 mm) was used as the counter electrode. A Pt wire (Nilaco corp., >99.98%, diameter: 1.0 mm) was employed as the quasi-reference electrode. The potential of the reference electrode was calibrated with reference to a dynamic  $K^+/K$  potential, which was prepared by the electrodeposition of K metal on a Ag wire. Galvanostatic electrolysis was conducted with various  $K_2SiF_6$  concentrations and current densities. The electrolyzed samples were washed in hot distilled water at 333 K for 24 h to remove the adhered salt on the deposits and dried under vacuum for 12 h. The samples were analyzed by SEM (Keyence Corp., VE-8800), energy dispersive X-ray spectroscopy (EDX; AMETEK Co. Ltd., EDAX Genesis APEX2), X-ray diffraction (XRD; Rigaku Corp., Ultima IV, Cu-K $\alpha$  line), and Raman spectroscopy (Tokyo Instruments Corp., Nanofinder30). For the cross-sectional SEM observations, the samples were embedded in acrylic resin and polished with emery paper and buffing compound. The impurity concentrations in the Si deposits were analyzed by GD-MS (Thermo Electron Corp., VG9000).

### 3. Results and Discussion

#### 3.1 Sample preparation

The galvanostatic electrolysis was conducted using a Ag wire electrode at various cathodic current densities from 10 to 500 mA cm<sup>-2</sup> in molten KF–KCl containing 0.5, 2.0, 3.5, and 5.0 mol%  $K_2SiF_6$ . Here, the reduction current is expressed as a positive value. In the electrolysis, the electric charge was fixed to 60 C (186 C cm<sup>-2</sup>). Figure 1 compares representative potential transient curves during the galvanostatic electrolysis at 38.8, 77.6, 155, and 310 mA cm<sup>-2</sup> in KF–KCl– $K_2SiF_6$  (2.0 mol%). In our previous study [16], deposition of Si and formation of K metal fog were found to occur from around 0.8 V and

0.2 V vs.  $K^+/K$ , respectively, from cyclic voltammetry. At the current densities of 38.8 and 77.6  $\text{mA cm}^{-2}$ , the potentials are around 0.8 V and 0.6 V, respectively, indicating that only Si deposition occurs. At higher current densities of 155 and 310  $\text{mA cm}^{-2}$ , the observed potentials are considerably negative and fluctuated in the potential range of K metal fog formation. In particular, at 310  $\text{mA cm}^{-2}$ , the potential is more negative than the deposition potential of K metal. Since these current densities are higher than the diffusion limiting current of  $\text{Si(IV)}$  ion, both the Si deposition and the K metal fog formation proceed simultaneously at the electrode. Under such condition, the adhesion of Si deposits becomes very poor and the detachment of deposits frequently occurs. Since the effective electrode area changes intermittently, the potential fluctuates.

\*\*\* Fig. 1 \*\*\*

### 3.2 Morphology of Si deposits

Figure 2 shows the optical microscope images of the electrolyzed samples after washing treatment. When the electrolysis was conducted at high current densities of 155 and 310  $\text{mA cm}^{-2}$  in  $\text{KF-KCl-K}_2\text{SiF}_6$  (0.5 mol%), no deposit remained on the Ag substrate. Except for these two samples, the deposition of crystalline Si was confirmed by XRD and Raman spectroscopy. Generally, the surface morphology is observed to become smoother as the current density decreased. The deposits obtained in the melt containing 5.0 mol%  $\text{K}_2\text{SiF}_6$  were found to exhibit rough surfaces.

Figure 3 shows the cross-sectional SEM images of the samples. Adherent, compact, and smooth Si films with a thickness of 50  $\mu\text{m}$  were electrodeposited at 77.6 and 155  $\text{mA cm}^{-2}$  in  $\text{KF-KCl}$  containing 2.0 and 3.5 mol%  $\text{K}_2\text{SiF}_6$  (Fig. 4). At higher current densities, nodular and coral-like Si is observed. Specifically, obvious porous structures are obtained

from electrolysis performed at current densities exceeding  $310 \text{ mA cm}^{-2}$ , as shown in the SEM images in Fig. 5. At lower current densities, the deposits are not homogeneous, and a flat Si layer is not obtained. At a high  $\text{K}_2\text{SiF}_6$  concentration of 5.0 mol%, porous and coral-like Si is observed, especially at higher current densities. In contrast, no deposition or partial removal of the Si layer occurred at a low  $\text{K}_2\text{SiF}_6$  concentration of 0.5 mol%.

\*\*\* Fig. 2 \*\*\*

\*\*\* Fig. 3 \*\*\*

\*\*\* Fig. 4 \*\*\*

\*\*\* Fig. 5 \*\*\*

Based on the SEM images presented in Fig. 3, the relationship between the electrolysis conditions and morphology of Si deposits is graphically drawn in Fig. 6. In this figure, the stars indicate the experimental electrolysis conditions, and the dashed boundaries are drawn between the stars. The optimum conditions for the electrodeposition of adherent, compact, and smooth Si layers are intermediate  $\text{K}_2\text{SiF}_6$  concentrations (2.0–3.5 mol%) and current densities ( $50\text{--}200 \text{ mA cm}^{-2}$ ). The morphologies of the Si deposits are explained below.

At high current densities, the morphology of the Si film changes from compact and smooth to nodular or coral-like. Electrolysis at high current densities increases concentration gradient of Si ions in the diffusion layer. As a result, Si deposition proceeds preferentially at convex parts of the deposited Si. Thus, the morphology becomes nodular or coral-like. At very low current densities, the Si layer on the Ag wire substrate has an uneven thickness, which is probably attributable to the uneven current distribution on the electrode: a thicker film forms on the side closest to the counter electrode, and a thinner



film forms on the opposite side. Hence, one has to pay special attention to the current distribution for the Si deposition in this melt. A possible technical measure to achieve the even current distribution is the placement of anodes so as to surround the cathode.

The formation of porous and coral-like Si layers at high  $\text{K}_2\text{SiF}_6$  concentrations results from the intermediate state of the Si ions. Figure 7 presents the differential pulse voltammograms for a Ag flag electrode in molten  $\text{KF-KCl-K}_2\text{SiF}_6$  (blank, 0.5, 2.0, 3.5, and 5.0 mol%) at 923 K. At a low concentration of 0.5 mol%, a single wave from Si(IV) to Si(0) is observed, which agrees with the results of our previous study [16]. In contrast, the separation of the reduction wave into two peaks becomes increasingly obvious as the  $\text{K}_2\text{SiF}_6$  concentration is increased. This behavior suggests the high stability of the intermediate states of the Si ions, such as Si(II), at high  $\text{K}_2\text{SiF}_6$  concentrations. At the low  $\text{K}_2\text{SiF}_6$  concentration of 0.5 mol%, no deposit is obtained at high current density. In this case, the electrode potential becomes so negative that K metal is codeposited, as shown in Fig. 1. The deposited Si likely dissociates from the Ag substrate because of the formation of liquid K metal or may be removed by  $\text{H}_2$  gas generated during the washing;  $\text{H}_2$  gas is evolved by the reaction of the K metal with water.

Furthermore, the diagram on the types of polycrystalline electrodeposits against overpotential and current density for the various bulk concentrations is of great interest. In aqueous solution systems, the relationship has been discussed using the so-called Winand diagram [17–19] which gives the fields of stability of Fischer's types of electrodeposits [20] as a function of two main parameters: the ratio of current density to the diffusion limiting current density, and the inhibition such as organic additives, exchange current density, and hydrogen overvoltage. The dependence of morphology on mass transfer, nucleation, and crystal growth would provide an instruction to elucidate

the electrocrystallization process even in high-temperature molten salts. Since the accurate overpotential is unknown for the present data, the illustration and interpretation of the diagram are interesting future tasks.

\*\*\* Fig. 6 \*\*\*

\*\*\* Fig. 7 \*\*\*

### 3.3 Purity of Si deposits

For purity determination, a sample was prepared by galvanostatic electrolysis of a Ag plate (0.2-mm thickness) at  $100 \text{ mA cm}^{-2}$  for 50 min in molten  $\text{KF-KCl-K}_2\text{SiF}_6$  (2.0 mol%) at 923 K. The experimental setup was the same as the previous section. Figure 8 shows a cross-sectional SEM image of the Si deposits. Adherent, compact, and relatively smooth Si films with thicknesses of 70–80  $\mu\text{m}$  are formed on both sides of the Ag substrate. Compositional analysis by EDX revealed that the films consisted of 100 at% Si. Based on the electric charge and sample weights before and after electrolysis, the current efficiency is calculated to be 93.1%. The remaining current might relate to the reduction of  $\text{Si(IV)}$  ions to Si ions with lower oxidation state such as  $\text{Si(II)}$ .

Table 1 summarizes the GD-MS results of the deposited Si films. For comparison, the reported acceptable impurity levels for solar-grade Si (SOG-Si) are also listed [21–24]. The deposited Si films contain some impurities derived from stainless steel and Ag derived from the substrate. The concentrations of B and P, which are the two most problematic elements for solar cell applications, are 3.2 ppmw and 2.7 ppmw, respectively. Although these levels are not appropriate for solar cell application, the fact that relatively low levels were found in the initial experiment, which involved no special considerations to ensure purity, suggests the great potential of the proposed process.

\*\*\* Fig. 8 \*\*\*

\*\*\* Table 1 \*\*\*

## **Conclusion**

For the establishment of a novel Si plating process, the optimum conditions for the electrodeposition of adherent, compact, and smooth Si layers in molten  $\text{KF-KCl-K}_2\text{SiF}_6$  at 923 K were investigated. Galvanostatic electrolysis with a Ag wire was conducted with various  $\text{K}_2\text{SiF}_6$  concentrations (0.5, 2.0, 3.5, and 5.0 mol%) and current densities ( $10\text{--}500\text{ mA cm}^{-2}$ ). Cross-sectional SEM observations of the deposits revealed that relatively compact and smooth Si layers are obtained at intermediate  $\text{K}_2\text{SiF}_6$  concentrations (2.0–3.5 mol%) and current densities ( $50\text{--}200\text{ mA cm}^{-2}$ ). The B and P impurities in the produced Si films were present at levels of a few ppm levels.

## **Acknowledgments**

This study was partly supported by the Core Research for Evolutionary Science and Technology (CREST) of the Japan Science and Technology Agency (JST).

## Reference

1. Y. Takeda, R. Kanno, and O. Yamamoto, *J. Electrochem. Soc.*, **128**, 1221 (1981).
2. M. Bechelany, J. Elias, P. Brodard, J. Michler, and L. Philippe, *Thin Solid Films*, **520**, 1895 (2012).
3. S. Z. E. Abedin, N. Borissenko, and F. Endres, *Electrochem. Commun.*, **6**, 510 (2004).
4. Y. Nishimura, Y. Fukunaka, T. Nishida, T. Nohira, and R. Hagiwara, *Electrochem. Solid-State Lett.*, **11**, D75 (2008).
5. G. M. Rao, D. Elwell, and R. S. Feigelson, *J. Electrochem. Soc.*, **127**, 1940 (1980).
6. G. M. Rao, D. Elwell, and R. S. Feigelson, *J. Electrochem. Soc.*, **128**, 1708 (1981).
7. D. Elwell, *J. Crystal Growth*, **52**, 741 (1981).
8. D. Elwell and R. S. Feigelson, *Sol. Energ. Mat.*, **6**, 123 (1982).
9. D. Elwell, *J. Appl. Electrochem.*, **18**, 15 (1988).
10. U. Cohen and R. A. Huggins, *J. Electrochem.*, **123**, 381 (1976).
11. G. M. Haarberg, L. Famiyeh, A. M. Martinez, and K. S. Osen, *Electrochim. Acta*, **100**, 226 (2013).
12. L. P. Cook and H. F. McMurdie, *Phase Diagrams for Ceramists vol. VII*, The American Ceramic Society Inc., 509 (1989).
13. A. A. Andriiko, E. V. Panov, O. I. Boiko, B. V. Yakovlev, and O. Ya. Borovik, *Rus. J. Electrochem.*, **33**, 1343 (1997).
14. K. Maeda, K. Yasuda, T. Nohira, R. Hagiwara, and T. Homma, *ECS Transactions, Molten Salts and Ionic Liquids*, **64**(4), 285 (2014).

15. T. Nohira, K. Maeda, K. Yasuda, R. Hagiwara, and T. Homma, Proceeding of 10th International Conference on Molten Salt Chemistry and Technology (MS10) and 5th Asian Conference on Molten Salts Chemistry and Technology (AMS5), Shenyang, China, 10–14 June, 2015, p. 70.
16. K. Maeda, K. Yasuda, T. Nohira, R. Hagiwara, and T. Homma, *J. Electrochem. Soc.*, **162**, D444 (2015).
17. R. Winand, *Mem. Scient. Revue Metall.*, **58**, 25 (1961).
18. R. Winand, *Hydrometallurgy*, **29**, 567 (1992).
19. R. Winand, *Electrochim. Acta*, **39**, 1091 (1994).
20. H. Fischer, *Elektrolytische Abscheidung und Elektrokristallisation von Metallen*, p. 729, Springer Verlag, Berlin (1954).
21. Y. Kato, N. Yuge, S. Hiwasa, H. Terashima, and F. Aratani, *Materia Japan*, **41**, 54 (2002).
22. M. A. Martorano, J. B. F. Neto, T. S. Oliveira, and T. O. Tsubaki, *Mater. Sci. Eng. B*, **176**, 217 (2011).
23. R. H. Hopkins and A. Rohatgi, *J. Crystal Growth*, **75**, 67 (1986).
24. J. R. Davis, Jr., A. Rohatgi, R. H. Hopkins, P. D. Blais, P. Rai-Choudhury, J. R. McCormick, and H. C. Mollenkopf, *IEEE Trans. Electron Devices*, **27**, 677 (1980).

### Figure captions

- Fig. 1 Potential shift during galvanostatic electrolysis on a Ag wire in KF–KCl–K<sub>2</sub>SiF<sub>6</sub> (2.0 mol%) at 923 K.
- Fig. 2 Optical microscope images of the samples obtained by galvanostatic electrolysis on a Ag wire in molten KF–KCl–K<sub>2</sub>SiF<sub>6</sub> at 923 K.
- Fig. 3 Cross-sectional SEM images of the samples obtained by galvanostatic electrolysis on a Ag wire in molten KF–KCl–K<sub>2</sub>SiF<sub>6</sub> at 923 K.
- Fig. 4 Cross-sectional SEM images of the samples obtained by galvanostatic electrolysis of Ag wire electrodes at 77.6 mA cm<sup>-2</sup> in molten KF–KCl–K<sub>2</sub>SiF<sub>6</sub> ((a) 2.0 mol% and (b) 3.5 mol%) at 923 K.
- Fig. 5 Cross-sectional SEM images of the samples obtained by galvanostatic electrolysis of Ag wire electrodes at 466 mA cm<sup>-2</sup> in molten KF–KCl–K<sub>2</sub>SiF<sub>6</sub> ((a) 2.0 mol% and (b) 5.0 mol%) at 923 K.
- Fig. 6 Relationship between the electrolysis conditions and the morphology of the Si deposits.
- Fig. 7 Differential pulse voltammograms for a Ag flag electrode in molten KF–KCl–K<sub>2</sub>SiF<sub>6</sub> (blank, 0.5, 2.0, 3.5, and 5.0 mol%) at 923 K.
- Fig. 8 A cross-sectional SEM image of the sample obtained by galvanostatic electrolysis of a Ag plate electrode at 100 mA cm<sup>-2</sup> for 50 min in molten KF–KCl–K<sub>2</sub>SiF<sub>6</sub> (2.0 mol%) at 923 K.

Table 1 Acceptable impurity levels for SOG-Si [21–24] and impurity contents determined by GD-MS for the sample obtained by galvanostatic electrolysis of an Ag plate at  $100 \text{ mA cm}^{-2}$  for 50 min in molten  $\text{KF-KCl-K}_2\text{SiF}_6$  (2.0 mol%) at 923 K.

Element	Acceptable levels for SOG-Si / ppmw			Impurity content in Si deposit / ppmw
	[21]	[22]	[23,24]	
B	0.1–0.3	0.1–10	—	3.2
Al	< 0.06	0.005–0.05	—	0.8
P	< 0.1	0.02–2	—	2.7
K	—	—	—	< 2
Ca	—	< 2	—	< 1
Ti	< $4 \times 10^{-5}$	< 1	< $1 \times 10^{-4}$	< 0.1
Cr	—	—	< $4 \times 10^{-3}$	5.1
Mn	—	—	< $8 \times 10^{-3}$	1.8
Fe	< 0.007	< 1	< 0.02	5.0
Ni	—	—	< 0.3	11
Cu	—	—	< 20	1.8
Mo	—	—	< $7 \times 10^{-5}$	0.6
Ag	—	—	—	76
Pt	—	—	—	< 0.5

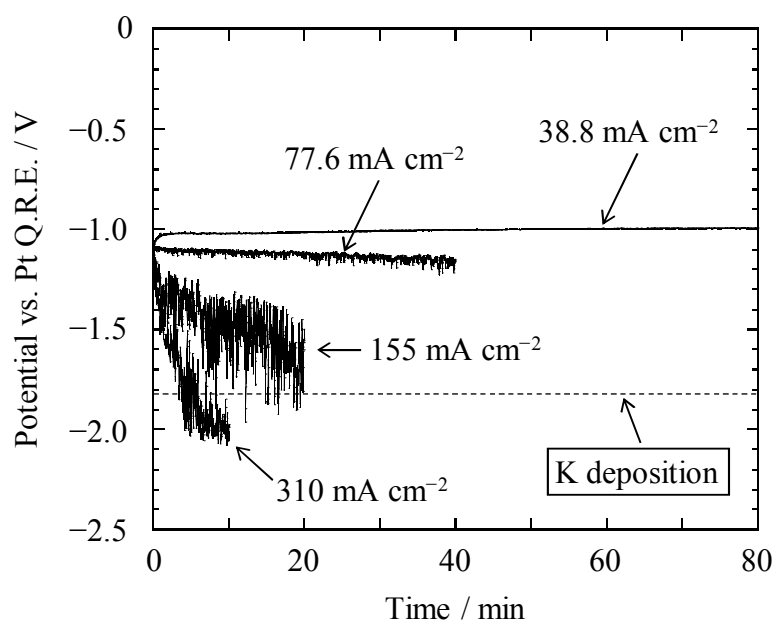
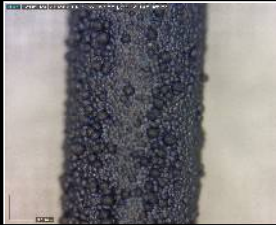


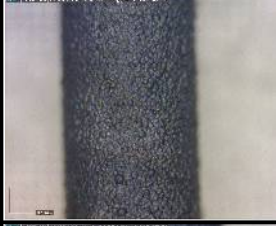
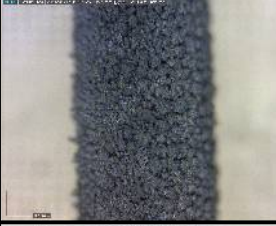
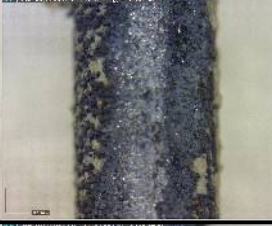

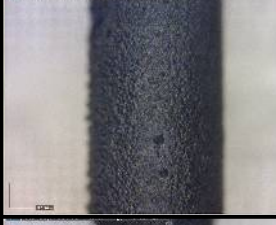
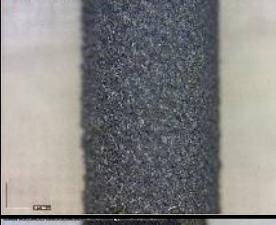



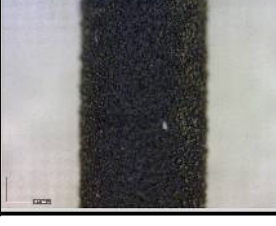



Fig. 1 Potential shift during galvanostatic electrolysis on a Ag wire in KF-KCl-K<sub>2</sub>SiF<sub>6</sub> (2.0 mol%) at 923 K.



	0.5 mol%	2.0 mol%	3.5 mol%	5.0 mol%
310 $\text{mA cm}^{-2}$	No deposit			
155 $\text{mA cm}^{-2}$				
77.6 $\text{mA cm}^{-2}$				
38.8 $\text{mA cm}^{-2}$				

1 mm

Fig. 2 Optical microscope images of the samples obtained by galvanostatic electrolysis on a Ag wire in molten  $\text{KF-KCl-K}_2\text{SiF}_6$  at 923 K.

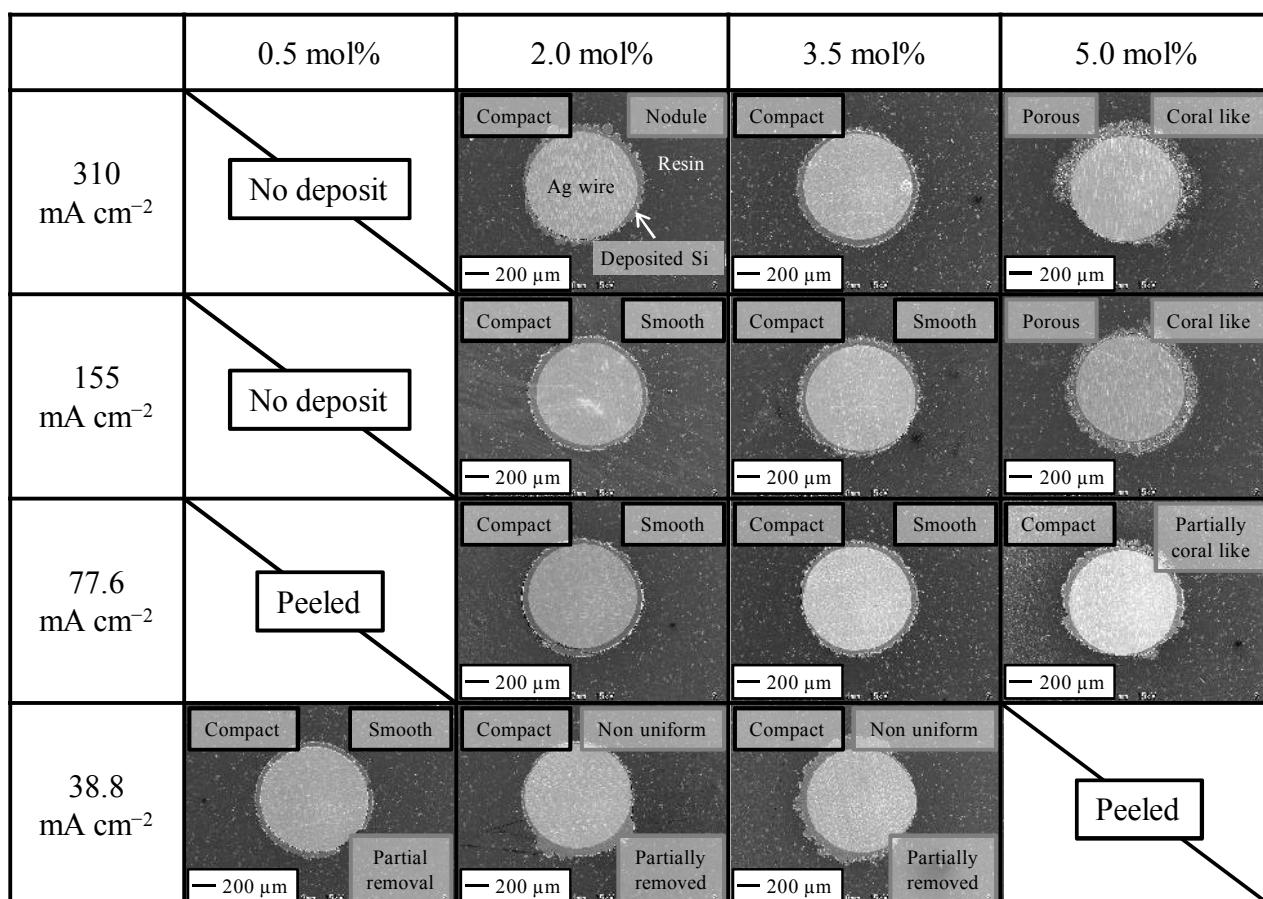
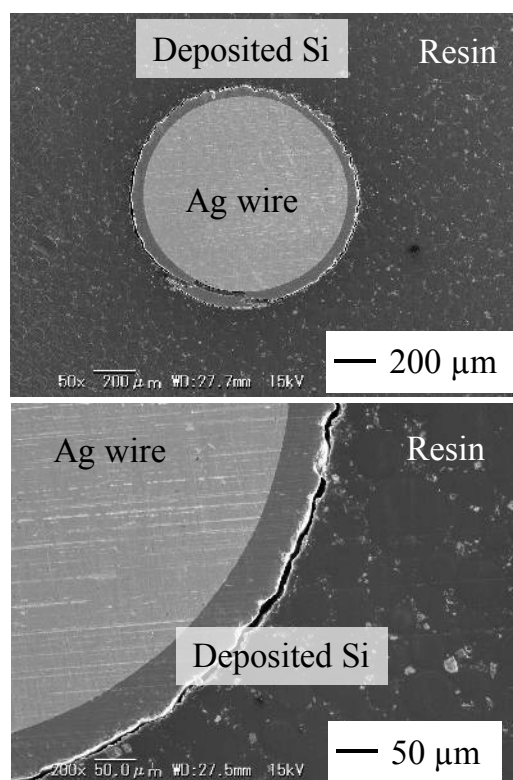


Fig. 3 Cross-sectional SEM images of the samples obtained by galvanostatic electrolysis on a Ag wire in molten  $\text{KF-KCl-K}_2\text{SiF}_6$  at 923 K.

(a) 2.0 mol%



(b) 3.5 mol%

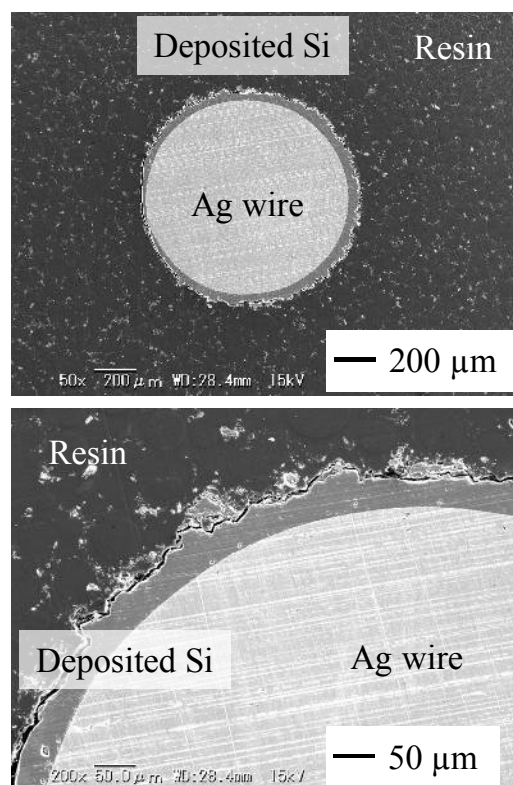
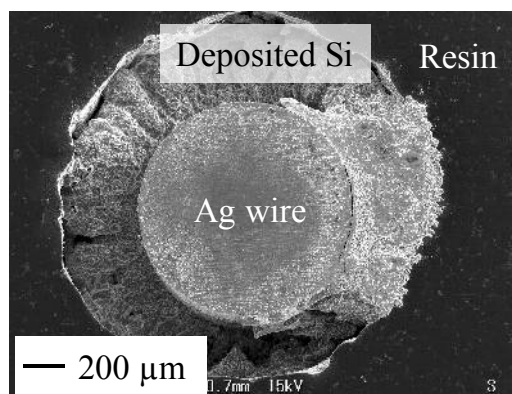


Fig. 4 Cross-sectional SEM images of the samples obtained by galvanostatic electrolysis of Ag wire electrodes at  $77.6 \text{ mA cm}^{-2}$  in molten  $\text{KF-KCl-K}_2\text{SiF}_6$  ((a) 2.0 mol% and (b) 3.5 mol%) at 923 K.

(a) 2.0 mol%



(b) 5.0 mol%

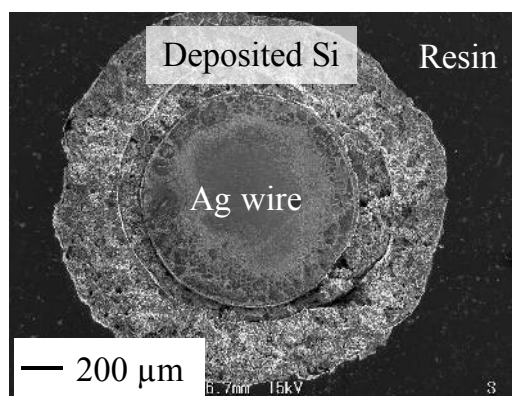


Fig. 5 Cross-sectional SEM images of the samples obtained by galvanostatic electrolysis of Ag wire electrodes at  $466 \text{ mA cm}^{-2}$  in molten  $\text{KF-KCl-K}_2\text{SiF}_6$  ((a) 2.0 mol% and (b) 5.0 mol%) at 923 K.

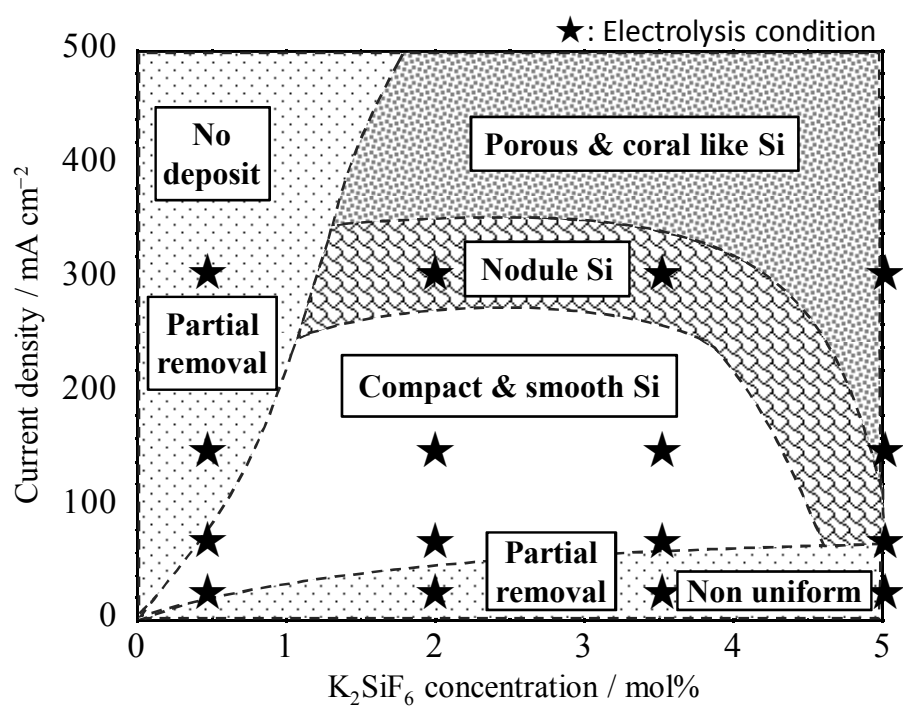


Fig. 6 Relationship between the electrolysis conditions and the morphology of the Si deposits.

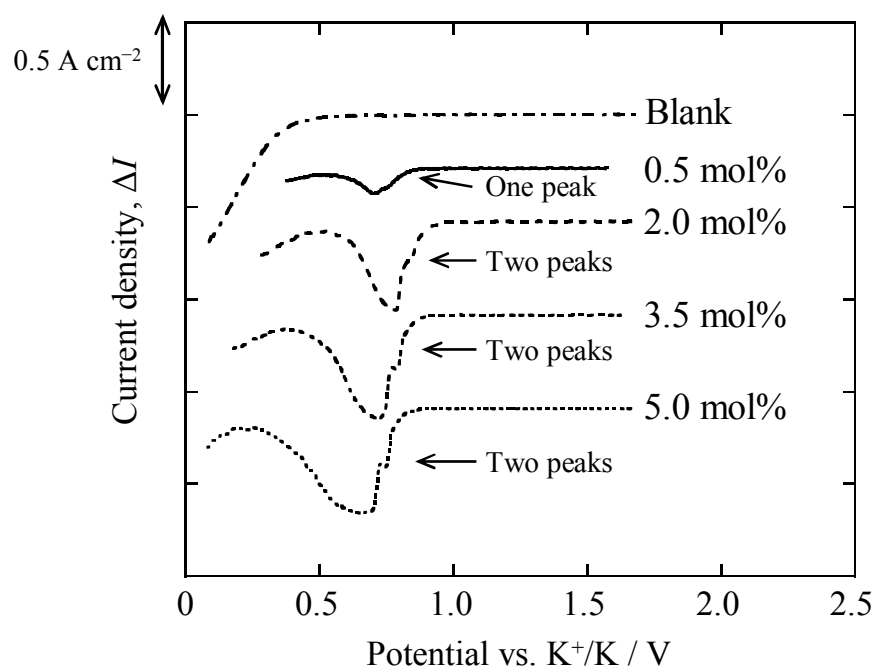


Fig. 7 Differential pulse voltammograms for a Ag flag electrode in molten  $\text{KF-KCl-K}_2\text{SiF}_6$  (blank, 0.50, 2.0, 3.5, and 5.0 mol%) at 923 K.

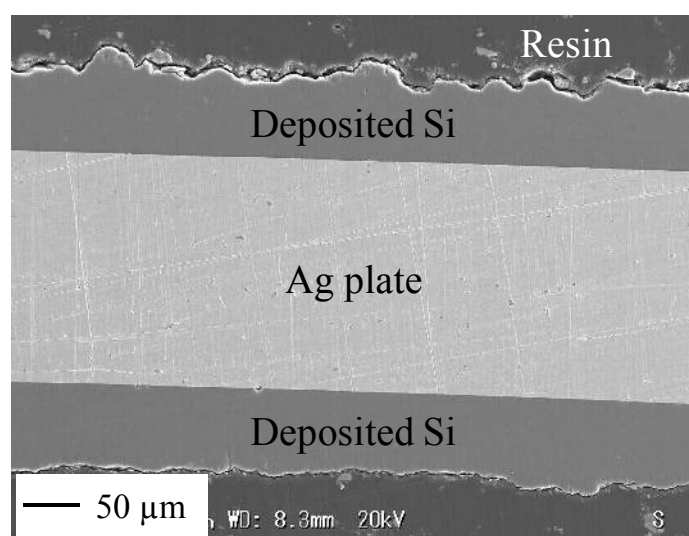


Fig. 8 A cross-sectional SEM image of the sample obtained by galvanostatic electrolysis of a Ag plate electrode at  $100 \text{ mA cm}^{-2}$  for 50 min in molten  $\text{KF-KCl-K}_2\text{SiF}_6$  (2.0 mol%) at 923 K.